Rescattering effects in soft-x-ray generation by laser-assisted electron-ion recombination

Dejan B. Milošević[1,*] and Fritz Ehlotzky[2,†]
[1]*Faculty of Science and Mathematics, Department of Physics, University of Sarajevo, Zmaja od Bosne 35, 71000 Sarajevo, Bosnia and Hercegovina*
[2]*Institute for Theoretical Physics, University of Innsbruck, Technikerstrasse 25, A-6020 Innsbruck, Austria*
(Received 31 August 2001; published 19 March 2002)

Laser-assisted electron-ion recombination is investigated with an emphasis on the spectrum of the emitted high-energy photons and its modification due to the recollision of the incident electron and the ion. Numerical results for the soft-x-ray power spectra, added up over all intermediate laser photon channels, are presented as a function of the incident electron energy for different laser field intensities. For strong laser fields, maxima, and additional structures are found in these spectra for incident electron energies of the order of magnitude of the ponderomotive energy. We show that the laser-assisted electron-ion recombination, that includes the rescattering of the electron at the ion before the recombination, is a process complementary to the well-known processes of high-order harmonic generation and high-order above-threshold ionization. All these processes can be explained, using the three-step scenario. A semiclassical analysis is presented which shows that for the laser-assisted electron-ion recombination real solutions of the saddle-point equations exist, contrary to what is found with high-order harmonic generation and high-order above-threshold ionization when only complex solutions are permitted. For low incoming electron energies, the cutoff of the emitted soft-x-ray photon energies, including the process of rescattering, is higher than in the case of the direct recombination process. The height of the rescattering plateau is 6–7 orders of magnitude lower than that of the direct process. However, for higher incident electron energies we obtain the unexpected result that the difference between the height of the rescattering plateau and the height of the direct plateau can be less than one order of magnitude.

DOI: 10.1103/PhysRevA.65.042504 PACS number(s): 32.30.Rj, 34.50.Rk, 34.80.Lx, 32.80.Wr

I. INTRODUCTION

The processes that take place during the interaction of a strong laser field with matter are presently studied very intensively [1–4]. The generation of coherent, extreme ultraviolet radiation and of soft x rays is currently a topic of great practical importance [5–8]. Such radiation can be produced by the laser heating of plasmas. Among the processes, that are responsible for high-energy photoproduction, we find: high-order harmonic generation (HHG) [9,10], laser-induced bremsstrahlung [11], laser-assisted x-ray–atom scattering [8,12], and laser-assisted electron-ion recombination (LAR) [13,14]. The present paper is devoted to the investigation of LAR and to its relation to HHG and the above-threshold ionization (ATI).

The history of electron-ion recombination, a process that is very important in plasma physics and astrophysics, goes back to 1923 (for an excellent review see [15]). A special case of this process is the radiative recombination in which the electron-ion recombination is made possible through the transfer of energy and momentum from the free electron to the photon as a third body. In most of the papers devoted to radiative recombination [16] the laser field is weak and thus only the one-photon LAR process is considered. Only very recently the multiphoton LAR process was analyzed in more detail [13,14,17].

In Refs. [13,14] the direct LAR process is considered: An incoming electron with the momentum $\mathbf{p}_i$ and the kinetic energy $E_{\mathbf{p}_i}$ recombines with the ion to yield the bound atomic state of the energy E_B. During this process, a high-energy photon with frequency $\omega_{\mathbf{K}}$ is emitted while n photons are exchanged with a laser field that has a low-frequency ω and a high intensity I. The ponderomotive energy of the electron in the laser field is $U_P=(e^2/2m)(1/T)\int_0^T dt\mathbf{A}^2(t)$, where $\mathbf{A}(t)$ is the vector potential of the laser field and $T=2\pi/\omega$ is the field period. In Ref. [13] it was found that the maximum energy of the emitted x rays is

$$\hbar\omega_{\mathbf{K},\max}=E_{\mathbf{p}_i}+2U_P+|E_B|+2\sqrt{2E_{\mathbf{p}_i}U_P}. \tag{1}$$

A similar expression for the minimum energy, which differs from Eq. (1) only by the sign on the left the square root, was also presented in Ref. [13]. This ''semiclassical'' result for the allowed interval of frequencies $\omega_{\mathbf{K}}$ is applicable to high energies of the incoming electron. For lower energies, with $E_{\mathbf{p}_i}<2U_P$ (the so-called ''slow electron regime'' of Ref. [14]), the minimum ''semiclassical'' energy is $\hbar\omega_{\mathbf{K},\max}=|E_B|$ if the electron velocity is parallel to the laser polarization. However, it can happen that the incoming electron first scatters at the ionic potential, then moves in the laser field, and, finally, after the laser field has changed its sign, the electron may come back to the nucleus and recombines. We shall denote this process as SLAR where ''*S*'' stands for ''scattering.'' We shall show in this paper that in case of low incoming electron energies the cutoff of the emitted soft-x-ray energies for the SLAR process can be larger than that given by Eq. (1).

The SLAR process, mentioned above, belongs together with HHG and high-order above-threshold ionization (HATI)

*Email address: milo@bih.net.ba
†Email address: Fritz.Ehlotzky@uibk.ac.at

to the class of the three-step processes [18–21]. Both, in HHG and HATI the atom is first ionized, absorbing more photons than it is necessary for ionization (this is the so-called above-threshold ionization). Depending on the instant of time at which the electron tunnels out, it may be driven back to the ionic core by the laser field (the second step) where, in the third step, it may recombine and release its energy by the emission of a single high-energy photon (HHG) or it may (re)collide with the ion and move away with a final energy $E_{\mathbf{p}_f}$ (HATI). HHG includes the (direct) recombination process [14]. The maximum emitted harmonic photon energy is given by the well-known cutoff law: $\hbar\omega_{\mathrm{H,max}}=|E_B|+3.17U_P$ (see [9] and references therein). Comparing this cutoff law with that given by Eq. (1) for $E_{\mathbf{p}_i}\ll U_P$: $\hbar\omega_{\mathbf{K},\mathrm{max}}\approx|E_B|+2U_P$, we see that the HHG cutoff is higher. The importance of HATI was confirmed both experimentally [22–24] and theoretically [25–28]. The cutoff law for this process is given by $E_{\mathbf{p}_f,\mathrm{max}}=10U_P$. If the HATI process becomes modified such that initially an x-ray photon is absorbed, then this process, according to the reciprocity theorem [29], may be considered as the time-reversed counterpart of our SLAR process [30]. Therefore, we can expect that for $E_{\mathbf{p}_i}<10U_P$ the SLAR process becomes important and should be investigated in more detail.

The outline of our paper is as follows. In Sec. II we present the *S*-matrix theory that includes both, the direct and the (re)scattering LAR process. In Refs. [13,14] there is no detailed analysis of the dependence of the probability of the LAR process on the incoming electron energy and on the laser field intensity. Therefore, in Sec. III we present numerical results for the direct LAR process, with emphasis on its dependence on the incident electron energy. In Sec. IV we present our numerical results that include both the direct LAR and the SLAR processes. A semiclassical analysis of these processes is given in Sec. V. Finally, our conclusions are presented in Sec. VI. Throughout the paper we shall use SI units. Sometimes we shall present our results in atomic units ($e=\hbar=m=1$).

II. THEORY

The process of direct recombination of an electron with an ion in the presence of a strong laser field, followed by the emission of an x-ray photon having the wave vector $\mathbf{K}$, frequency $\omega_{\mathbf{K}}$ and unit polarization vector $\hat{\mathbf{e}}_{\mathbf{K}}$, was described in [13,14]. We want to consider here how this process is modified if the electron scatters first at the ionic potential, then is driven by the laser field and, as soon as the laser field changes its sign, it returns to the ion and recombines emitting an x-ray photon. This is a variant of the three-step model [18] developed in the context of HHG, but applied also to HATI [25–28] and, moreover, in a unified approach [19–21].

Our starting point will be similar to the one in Ref. [12], in which we considered laser-assisted x-ray–atom scattering, and to Refs. [27,28] where Coulomb and rescattering effects in above-threshold ionization were considered. We begin with the following general form of the *S* matrix,

$$S_{fi}=i\hbar\lim_{t'\to\infty}\lim_{t\to-\infty}\langle\Phi_{\mathrm{out}}(t')|G^{(+)}(t',t)|\Phi_{\mathrm{in}}(t)\rangle. \quad (2)$$

The total Green's operator $G^{(+)}$ corresponds to the total Hamiltonian

$$H=H_0+e\mathbf{r}\cdot\mathbf{E}_X(\mathbf{r},t),\quad H_0=\frac{\mathbf{p}^2}{2m}+V_A+e\mathbf{r}\cdot\mathbf{E}_L(t), \quad (3)$$

where $e\mathbf{r}\cdot\mathbf{E}_X(\mathbf{r},t)$ describes the interaction of the atom with the x-ray field (in the length gauge), $\mathbf{p}^2/(2m)$ represents the kinetic energy operator, V_A is the atomic binding potential, and $e\mathbf{r}\cdot\mathbf{E}_L(t)$ is the laser-atom interaction (using the length gauge and the dipole approximation). We shall consider the x-ray radiation field as quantized [12,13,31,32], namely,

$$\mathbf{E}_X(\mathbf{r},t)=\mathbf{E}_X^{(+)}(\mathbf{r},t)+\mathbf{E}_X^{(-)}(\mathbf{r},t),$$

$$\mathbf{E}_X^{(+)}(\mathbf{r},t)=iC_{\mathbf{K}}\hat{\mathbf{e}}_{\mathbf{K}}a_{\mathbf{K}}\exp[-i(\omega_{\mathbf{K}}t-\mathbf{K}\cdot\mathbf{r})],$$

$$\mathbf{E}_X^{(-)}(\mathbf{r},t)=-iC_{\mathbf{K}}\hat{\mathbf{e}}_{\mathbf{K}}a_{\mathbf{K}}^{\dagger}\exp[i(\omega_{\mathbf{K}}t-\mathbf{K}\cdot\mathbf{r})], \quad (4)$$

where $a_{\mathbf{K}}$ and $a_{\mathbf{K}}^{\dagger}$ are the photon annihilation and creation operators of the x-ray field, and $C_{\mathbf{K}}^2=\hbar\omega_{\mathbf{K}}/(2\varepsilon_0\mathcal{V})$ with $\mathcal{V}$ denoting the quantization volume. Our *in* state in Eq. (2) is the initial electron scattering state in the absence of the laser field (it is a plane wave with momentum $\mathbf{p}_i$, assuming V_A is only a short-range potential) multiplied by the vacuum state $|0_{\mathbf{K}}\rangle$ of the x-ray field. Our *out* state is the bound electron state (in the absence of the laser field) multiplied by the one-photon state $|1_{\mathbf{K}}\rangle$ for x rays. Using the Lippmann-Schwinger equation for the total Green's operator and the two relations $\langle\Phi_f^{(-)}(t)|=i\hbar\langle\Phi_{\mathrm{out}}(\infty)|G^{(+)}(\infty,t)$, $i\hbar G_0^{(+)}(t,-\infty)|\Phi_{\mathrm{in}}(-\infty)\rangle=|\Psi_{\mathbf{p}_i}^{(+)}(t)\rangle|0_{\mathbf{K}}\rangle$, as was done in [12,28,31], we find

$$S_{fi}=-\frac{i}{\hbar}\int_{-\infty}^{\infty}dt\langle\Phi_f^{(-)}(t)|e\mathbf{r}\cdot\mathbf{E}_X^{(-)}(\mathbf{r},t)|\Psi_{\mathbf{p}_i}^{(+)}(t)\rangle|0_{\mathbf{K}}\rangle, \quad (5)$$

where $|\Psi_{\mathbf{p}_i}^{(+)}(t)\rangle$ is the solution of the Schrödinger equation for the Hamiltonian H_0 of Eq. (3). We suppose that the atomic potential consists of a long-range Coulomb part V_C and a short-range part V_S, i.e., $V_A=V_C+V_S$. In order to investigate the electron scattering at the potential V_S we choose the following splitting of the Hamiltonian $H_0=(H_0-V_S)+V_S$, that leads to the Lippmann-Schwinger equation

$$|\Psi_{\mathbf{p}_i}^{(+)}(t)\rangle=|\psi_{\mathbf{p}_i,C}^{(+)}(t)\rangle+\int dt' G_0^{(+)}(t,t')V_S|\psi_{\mathbf{p}_i,C}^{(+)}(t')\rangle, \quad (6)$$

where the state $|\psi_{\mathbf{p}_i,C}^{(+)}(t)\rangle$ evolves from the *in* state of the electron under the action of the Green's operator $G_C^{(+)}$ that belongs to the Hamiltonian H_0-V_S: $|\psi_{\mathbf{p}_i,C}^{(+)}(t)\rangle=i\hbar G_C^{(+)}(t,-\infty)|\psi_{\mathrm{in}}(-\infty)\rangle$, with $|\Phi_{\mathrm{in}}(t)\rangle=|\psi_{\mathrm{in}}(t)\rangle|0_{\mathbf{K}}\rangle$. We approximate this state by the Volkov wave vector in the length gauge [14,27]

$$|\psi^{(+)}_{\mathbf{p}_i,C}(t)\rangle \approx |\chi_{\mathbf{p}_i}(t)\rangle = |\mathbf{p}_i + e\mathbf{A}(t)\rangle \times \exp\left\{-\frac{i}{\hbar}[\mathbf{p}_i\cdot\boldsymbol{\alpha}(t) + \mathcal{U}(t) + E_{\mathbf{p}_i}t]\right\}, \quad (7)$$

in which

$$\boldsymbol{\alpha}(t) = \frac{e}{m}\int^t dt'\,\mathbf{A}(t'),$$

$$\mathcal{U}(t) = \frac{e^2}{2m}\int^t dt'\,\mathbf{A}^2(t') = \mathcal{U}_1(t) + U_P t, \quad (8)$$

with $\mathbf{E}_L(t) = -\partial\mathbf{A}(t)/\partial t$, $E_{\mathbf{p}_i} = \mathbf{p}_i^2/(2m)$, $U_P = e^2\langle\mathbf{A}^2(t)\rangle/(2m)$, and $\mathcal{U}_1(t)$ the time periodic part of $\mathcal{U}(t)$. This ansatz is satisfactory within the strong-field approximation [33,34]. The influence of both the laser field and the Coulomb potential can be taken into account by using the improved Coulomb-Volkov state ansatz ([13,28] and references therein) instead of Eq. (7). According to the first reference in Ref. [28] we do not expect that the improved Coulomb-Volkov state ansatz will introduce qualitative changes in the final SLAR results so that we will keep the simpler ansatz (7). Our next approximation is to replace the intermediate Green's propagator $G_0^{(+)}$ in Eq. (6) by the Volkov Green's operator

$$G_L^{(+)}(t,t') = -\frac{i}{\hbar}\theta(t-t')\int d^3q\,|\chi_{\hbar\mathbf{q}}(t)\rangle\langle\chi_{\hbar\mathbf{q}}(t')|, \quad (9)$$

which is also the usual approximation within the strong-field approximation. Our final approximation [13] is to neglect the field dressing of the final state $|\Phi_f^{(-)}(t)\rangle$ in Eq. (5). We shall describe it by the atomic ground state multiplied by the one-photon state: $|\Phi_f^{(-)}(t)\rangle \approx |\psi_B\rangle\exp(-iE_Bt/\hbar)|1_{\mathbf{K}}\rangle$. Introducing all these approximations into Eq. (5) we obtain

$$\begin{aligned} S_{fi} = &-\frac{C_{\mathbf{K}}}{\hbar}\int_{-\infty}^{\infty} dt\,\exp\left[\frac{i}{\hbar}(E_B+\hbar\omega_{\mathbf{K}})t\right] \\ &\times\Bigg[\langle\psi_B|e\mathbf{r}\cdot\hat{\mathbf{e}}_{\mathbf{K}}e^{-i\mathbf{K}\cdot\mathbf{r}}|\mathbf{p}_i+e\mathbf{A}(t)\rangle \\ &\times\exp\left\{-\frac{i}{\hbar}[\mathbf{p}_i\cdot\boldsymbol{\alpha}(t)+\mathcal{U}(t)+E_{\mathbf{p}_i}t]\right\} \\ &-\frac{i}{\hbar}\int_{-\infty}^{t}dt'\int d^3q\langle\psi_B|e\mathbf{r}\cdot\hat{\mathbf{e}}_{\mathbf{K}}e^{-i\mathbf{K}\cdot\mathbf{r}}|\hbar\mathbf{q}+e\mathbf{A}(t)\rangle \\ &\times\exp\left\{-\frac{i}{2m\hbar}\int_{t'}^{t}dt''[\hbar\mathbf{q}+e\mathbf{A}(t'')]^2\right\} \\ &\times\langle\hbar\mathbf{q}+e\mathbf{A}(t')|V_S|\mathbf{p}_i+e\mathbf{A}(t')\rangle \\ &\times\exp\left\{-\frac{i}{\hbar}[\mathbf{p}_i\cdot\boldsymbol{\alpha}(t')+\mathcal{U}(t')+E_{\mathbf{p}_i}t']\right\}\Bigg]. \end{aligned} \quad (10)$$

The double integral over time in the above equation can be rearranged using the relation

$$\int_{-\infty}^{\infty}dt\int_{-\infty}^{t}dt'f(t,t') = \int_{-\infty}^{\infty}dt'\int_{t'}^{\infty}dt f(t,t') = \int_{-\infty}^{\infty}dt'\int_0^{\infty}d\tau f(t'+\tau,t'),$$

so that, writing t instead of t', we finally find

$$\begin{aligned} S_{fi} = &-\frac{C_{\mathbf{K}}}{\hbar}\int_{-\infty}^{\infty}dt\,\exp\Bigg\{\frac{i}{\hbar}[(E_B+\hbar\omega_{\mathbf{K}}-E_{\mathbf{p}_i}-U_P)t \\ &-\mathbf{p}_i\cdot\boldsymbol{\alpha}(t)-\mathcal{U}_1(t)]\Bigg\}\Bigg\{\langle\psi_B|e\mathbf{r}\cdot\hat{\mathbf{e}}_{\mathbf{K}}e^{-i\mathbf{K}\cdot\mathbf{r}}|\mathbf{p}_i+e\mathbf{A}(t)\rangle \\ &-\frac{i}{\hbar}\int_0^{\infty}d\tau\int d^3q\,\langle\psi_B|e\mathbf{r}\cdot\hat{\mathbf{e}}_{\mathbf{K}}e^{-i\mathbf{K}\cdot\mathbf{r}}|\hbar\mathbf{q}+e\mathbf{A}(t+\tau)\rangle \\ &\times\exp\left[-\frac{i}{\hbar}S(\mathbf{q};t,\tau)\right]\langle\hbar\mathbf{q}+e\mathbf{A}(t)|V_S|\mathbf{p}_i+e\mathbf{A}(t)\rangle\Bigg\}, \end{aligned} \quad (11)$$

where

$$S(\mathbf{q};t,\tau) = \int_t^{t+\tau}dt'\left\{\frac{[\hbar\mathbf{q}+e\mathbf{A}(t')]^2}{2m} - E_B - \hbar\omega_{\mathbf{K}}\right\} \quad (12)$$

is the semiclassical action [35,36]. The S-matrix element, written in the form of Eq. (11), has a simple physical interpretation. At some initial time t the electron can directly recombine into the ground state emitting an x-ray photon. This process is described by the first term in the curly bracket on the right-hand side of Eq. (11). The electron can also scatter on the potential V_S and propagate in the laser field from the instant of time t to time $t+\tau$ when it comes back to the nucleus and recombines by emitting an x-ray photon (this process is represented by the second term in the curly bracket given above). Having obtained this result, we can now solve the integral over the intermediate electron momenta $\hbar\mathbf{q}$ using the saddle-point method [12,27,28,31,35,36]. In general case, this integral can be presented as a Taylor expansion around the saddle point $\mathbf{q}=\mathbf{q}_s$ that contains powers of $\hbar/\tau$ (τ is the travel time) multiplied by the even derivatives over the intermediate electron momenta of the nonexponential subintegral term in Eq. (11) [36]. The main contribution comes from the zeroth-order term. This integral can be solved analytically for the Gaussian model, the zero-range potential model, and the hydrogenlike atoms model. Observing also the periodicity of the subintegral function in the S-matrix element, we obtain with $\varphi = \omega t$,

$$\begin{aligned} S_{fi} &= -\frac{C_{\mathbf{K}}}{\hbar}\int_{-\infty}^{\infty}dt\,\exp\left[\frac{i}{\hbar}(E_B+\hbar\omega_{\mathbf{K}}-E_{\mathbf{p}_i}-U_P)t\right]\mathcal{T}_{fi}(\varphi) \\ &= -2\pi C_{\mathbf{K}}\sum_n\,\delta(E_B+\hbar\omega_{\mathbf{K}}-E_{\mathbf{p}_i}-U_P-n\hbar\omega)T_{fi}(n), \end{aligned} \quad (13)$$

$$\mathcal{T}_{fi}(\varphi)=\sum_{n=-\infty}^{\infty}T_{fi}(n)e^{-in\varphi}=\exp\left\{-\frac{i}{\hbar}[\mathbf{p}_i\cdot\boldsymbol{\alpha}(\varphi)+\mathcal{U}_1(\varphi)]\right\}$$
$$\times\left\{\langle\psi_B|e\mathbf{r}\cdot\hat{\mathbf{e}}_{\mathbf{K}}e^{-i\mathbf{K}\cdot\mathbf{r}}|\mathbf{p}_i+e\mathbf{A}(\varphi)\rangle\right.$$
$$-\frac{i}{\hbar}\int_0^{\infty}d\tau\left(\frac{2\pi m}{i\hbar\tau}\right)^{3/2}\exp\left[-\frac{i}{\hbar}S(\mathbf{q}_s;\varphi,\omega\tau)\right]$$
$$\times\langle\psi_B|e\mathbf{r}\cdot\hat{\mathbf{e}}_{\mathbf{K}}e^{-i\mathbf{K}\cdot\mathbf{r}}|\hbar\mathbf{q}_s+e\mathbf{A}(\varphi+\omega\tau)\rangle$$
$$\left.\times\langle\hbar\mathbf{q}_s+e\mathbf{A}(\varphi)|V_S|\mathbf{p}_i+e\mathbf{A}(\varphi)\rangle\right\},\qquad(14)$$

where the stationary momentum $\hbar\mathbf{q}_s(t,\tau)=-(e/\tau)\int_t^{t+\tau}dt'\mathbf{A}(t')$ is the solution of the equation $\boldsymbol{\nabla}_{\mathbf{q}}S(\mathbf{q};t,\tau)=\mathbf{0}$. The matrix elements in Eq. (14) have a simple analytical form so that the T-matrix element $T_{fi}(n)=\int_0^{2\pi}d\varphi/2\pi\mathcal{T}_{fi}(\varphi)\exp(in\varphi)$ can be easily computed by performing the integration over the travel time τ and by using the fast Fourier transform method.

The density of states of the x-ray radiation emitted, quantized in a volume $\mathcal{V}$, is $\mathcal{V}/(2\pi c)^3\omega_{\mathbf{K}}^2d\omega_{\mathbf{K}}d\Omega_{\hat{\mathbf{K}}}$, while the density of the electron states [normalized to a plane wave $(2\pi\hbar)^{-3/2}\exp(i\mathbf{q}\cdot\mathbf{r})$] is $mp_idE_{\mathbf{p}_i}d\Omega_{\hat{\mathbf{p}}_i}$. Therefore, the differential rate for the emission of an x-ray photon [having its frequency within the interval $(\omega_{\mathbf{K}}-d\omega_{\mathbf{K}},\omega_{\mathbf{K}}+d\omega_{\mathbf{K}})$ and the polarization $\hat{\mathbf{e}}_{\mathbf{K}}$], into the solid angle $d\Omega_{\hat{\mathbf{K}}}$, during the recombination of an electron with initial energy $E_{\mathbf{p}_i}$ impinging from within the solid angle $d\Omega_{\hat{\mathbf{p}}_i}$, is given by ($T_p$ denotes the pulse duration time)

$$dw(\mathbf{K},\mathbf{p}_i)=\frac{1}{T_p}d\Omega_{\hat{\mathbf{K}}}dE_{\mathbf{p}_i}d\Omega_{\hat{\mathbf{p}}_i}\int_{\omega_{\mathbf{K}}-d\omega_{\mathbf{K}}}^{\omega_{\mathbf{K}}+d\omega_{\mathbf{K}}}d\omega_{\mathbf{K}}\frac{\mathcal{V}\omega_{\mathbf{K}}^2}{(2\pi c)^3}mp_i$$
$$\times(-2\pi C_{\mathbf{K}})^2\sum_n T_{fi}(n)$$
$$\times\delta(E_B+\hbar\omega_{\mathbf{K}}-E_{\mathbf{p}_i}-U_P-n\hbar\omega)$$
$$\times\sum_{n'}T_{fi}^*(n')\delta(E_B+\hbar\omega_{\mathbf{K}}-E_{\mathbf{p}_i}-U_P-n'\hbar\omega).\qquad(15)$$

The product of the δ functions is different from zero for $n=n'$. The first δ function can be eliminated on account of the relation $2\pi\hbar\delta(0)=T_p$ (for $T_p\to\infty$), while the second delta function disappears on account of the integration over $d\omega_{\mathbf{K}}$ and we obtain for the differential rate of the process of the emission of an x-ray photon in which n photons are exchanged with the laser field

$$dw(\mathbf{K},\mathbf{p}_i)=\frac{mp_i\omega_{\mathbf{K}}^3}{8\pi^2\varepsilon_0\hbar c^3}|T_{fi}(n)|^2d\Omega_{\hat{\mathbf{K}}}dE_{\mathbf{p}_i}d\Omega_{\hat{\mathbf{p}}_i},$$
$$n\hbar\omega=\hbar\omega_{\mathbf{K}}-|E_B|-E_{\mathbf{p}_i}-U_P,\qquad(16)$$

where the second relation in Eq. (16) expresses the energy conserving condition. The corresponding differential power spectrum is [13] $S(\mathbf{K},\mathbf{p}_i)=\hbar\omega_{\mathbf{K}}dw(\mathbf{K},\mathbf{p}_i)/(d\Omega_{\hat{\mathbf{K}}}dE_{\mathbf{p}_i}d\Omega_{\hat{\mathbf{p}}_i})$.

As in Ref. [13], we consider a configuration of the laser and x-ray fields and of the incoming electron such that $\hat{\mathbf{e}}_L=\hat{\mathbf{e}}_{\mathbf{K}}=-\mathbf{p}_i/p_i$, $p_i=|\mathbf{p}_i|$, so that $\mathbf{p}_i\cdot\boldsymbol{\alpha}(\varphi)=-p_i\alpha(\varphi)$. The quantity, which we shall evaluate in our examples, is $2\pi S$ where the factor 2π comes from the integration over the azimuthal angle of electron incidence. Moreover, we assume in our calculations that the laser field is monochromatic and linearly polarized with the electric field vector $\mathbf{E}_L(t)=E_0\hat{\mathbf{e}}_L\sin\omega t$, and with the photon energy $\hbar\omega=1.17$ eV [Nd: yttrium aluminum garnet (YAG) laser].

For the ground-state wave function we use either the one of the hydrogen atom $\psi_B(\mathbf{r})=\pi^{-1/2}\exp(-r)$ (in atomic units and $E_B=-0.5$ a.u.) or that of He that can be found in Ref. [37]. (This function for He is presented in an analytic form and was obtained in a nonrelativistic approximation by a series expansion in terms of atomic Slater orbitals. The binding energy for He is $E_B=-24.59$ eV.) For the short-range potential V_S we chose a potential of the form: $-(a+b/r)\exp(-\lambda r)$ [38]. In particular, in the case of the hydrogen atom, we took the Yukawa-type short-range potential $V_S=-\exp(-r)/r$, while for He we employed [39] $V_S(\mathbf{r})=-(2+1/r)\exp(-4r)$ (in a.u.). This form of the short-range potential for He is obtained by using the formula [40] $V_A(\mathbf{r})=\int d\mathbf{r}'|\psi_{\mathrm{He}^+}(\mathbf{r}')|^2/|\mathbf{r}-\mathbf{r}'|-Z/r$ where the first term represents the interaction of the ionized electron with the electron core cloud and Z is the nuclear charge. We have chosen these two simple examples (the case of e^--H^+ scattering modeled by the Yukawa-type potential may look unrealistic) having in mind that our aim is to obtain a qualitative picture of the electron-ion recombination process that takes place in a strong laser field.

III. DIRECT LAR PROCESS: INCIDENT ELECTRON ENERGY DEPENDENCE

The differential power spectrum for the direct LAR process is determined by a one-dimensional integral over an analytical expression and can be easily evaluated by numerical integration [13,14] or, even faster, using the fast Fourier transform method. The results obtained can be analyzed by the (semi)classical method, outlined in Refs. [13,14] and in Sec. V of our paper. We present here our results for the total emitted x-ray power in the direct LAR process for different laser field intensities as a function of the incident electron kinetic energy. The total power we define as $\int d\phi_i\int d\omega_{\mathbf{K}}S(\mathbf{p}_i,\mathbf{K})=2\pi\Sigma_nS(\mathbf{p}_i,\mathbf{K})$, where ϕ_i is the azimuthal angle of the incident electron and the integral over $d\omega_{\mathbf{K}}$ is replaced, using the energy conserving condition, by the sum over the number of exchanged photons. The other angles in the problem shall be fixed by the condition $\hat{\mathbf{e}}_{\mathbf{K}}=-\mathbf{p}_i/p_i=\hat{\mathbf{e}}_L$.

In Fig. 1 we present the results for the hydrogen atom as target for a Nd:YAG laser of the intensities 10^{12} W/cm^2, 10^{13} W/cm^2, and 10^{14} W/cm^2. The corresponding ponderomotive energies are 0.1048 eV, 1.048 eV, and 10.48 eV, re-

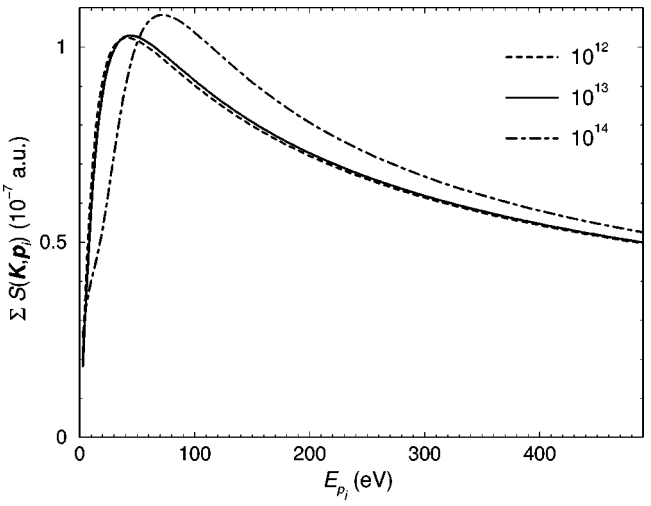

FIG. 1. The total power of the emitted x rays as a function of the incoming electron energy, for the hydrogen atom and a Nd:YAG laser of intensities 10^{12} W/cm^2 (dashed curve), 10^{13} W/cm^2 (solid curve), and 10^{14} W/cm^2 (dotted-dashed curve).

spectively. One can see that the total power increases with the decrease of the incident electron energy. The maxima appear at: $E_{\mathbf{p}_i}=41$ eV$=391U_P$ (for 10^{12} W/cm^2), $E_{\mathbf{p}_i}=44$ eV$=42U_P$ (for 10^{13} W/cm^2), and $E_{\mathbf{p}_i}=72$ eV $=6.87U_P$ (for 10^{14} W/cm^2). With a further decrease of $E_{\mathbf{p}_i}$, the total power rapidly decreases, after the maxima have been reached.

With an increasing laser field intensity, the maxima appear for lower values of $E_{\mathbf{p}_i}/U_P$. In addition, for lower values of $E_{\mathbf{p}_i}$ a more complicated structure in the total power appears with a minimum and an additional maximum. This can be seen in Fig. 2 where we present the results for H at the intensity 10^{15} W/cm^2 ($U_P=104.8$ eV), and for He at

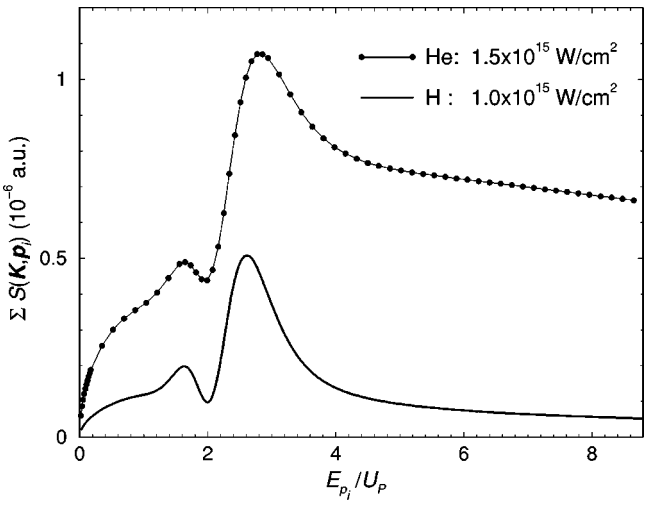

FIG. 2. The total power of the emitted x rays as a function of the incoming electron energy divided by the ponderomotive energy U_P, for H and the intensity 10^{15} W/cm^2 (bold solid line) and for He and the intensity 1.5×10^{15} W/cm^2 (solid line with filled circles). The laser photon energy is $\hbar\omega=1.17$ eV.

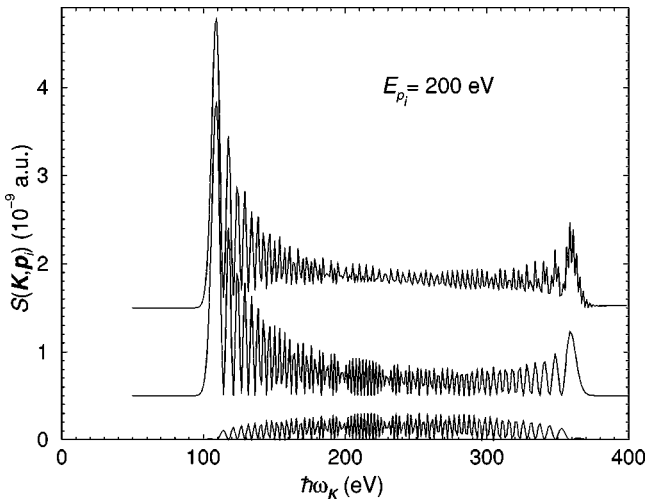

FIG. 3. Numerical results for the differential power spectrum as a function of the emitted x-ray energy for the hydrogen atom, a Nd:YAG laser of intensity 10^{14} W/cm^2 ($U_P=10.48$ eV), and the incident electron energy $E_{\mathbf{p}_i}=200$ eV. Top curve, the total result; middle curve, direct LAR only; bottom curve, SLAR only. The middle (top) curve is displaced up by 0.5 (1.5) units of the ordinate scale for increasing the visibility.

$I=1.5\times10^{15}$ W/cm^2. (Here I is taken as the saturation intensity for He according to [2]; with $U_P=157.3$ eV.) In this figure, the results are presented as a function of $E_{\mathbf{p}_i}$ divided by the corresponding value of the ponderomotive energy. The larger maximum occurs at $E_{\mathbf{p}_i}=272$ eV$=2.6U_P$ (for H) and $E_{\mathbf{p}_i}=440$ eV$=2.8U_P$ (for He), while the lower maximum appears at $E_{\mathbf{p}_i}=171$ eV$=1.63U_P$ (for H) and $E_{\mathbf{p}_i}=258$ eV$=1.64U_P$ (for He). From the results presented in Figs. 1 and 2 we conclude that the direct LAR process for high laser-field intensities is most efficient if the incident electron energy is of the order of magnitude of a few U_P.

IV. NUMERICAL RESULTS

We shall first present the results for the case in which the incoming electron energy is larger than $10U_P$. In this case, as we will see in the next section, the SLAR process is classically forbidden. In Fig. 3, on a linear scale, we present the numerical results for the differential power spectrum as a function of the emitted x-ray energy for the hydrogen atom, for a Nd:YAG laser of intensity 10^{14} W/cm^2, and for the incoming electron energy $E_{\mathbf{p}_i}=200$ eV$=19U_P$; $U_P=10.48$ eV. The results of direct LAR (the curve in the middle) show the characteristic oscillatory behavior [13] with pronounced maxima at both ends of the classically allowed region (105 eV$\leqslant\hbar\omega_{\mathbf{K}}\leqslant$364 eV). The lower curve shows the corresponding SLAR results, while the top curve shows the total result that is the coherent superposition of these two results. The middle and the top curves are shifted up for permitting a better visibility. The oscillatory character of both the direct LAR and the SLAR curves is similar, except that the SLAR curve does not exhibit pronounced maxima at the boundaries of the classically allowed region.

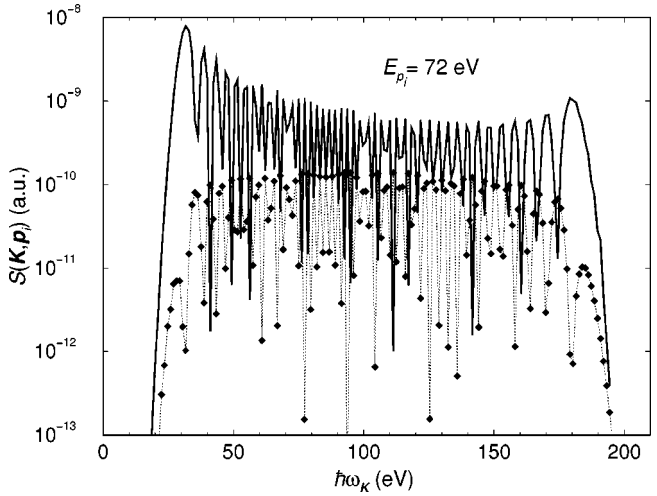

FIG. 4. Numerical results for the differential power spectrum for the same parameters as in Fig. 3 but for the incident electron energy $E_{\mathbf{p}_i}=72$ eV. The results for the direct LAR are presented by a solid line, while the results for SLAR only, are presented by a dotted line with filled diamonds.

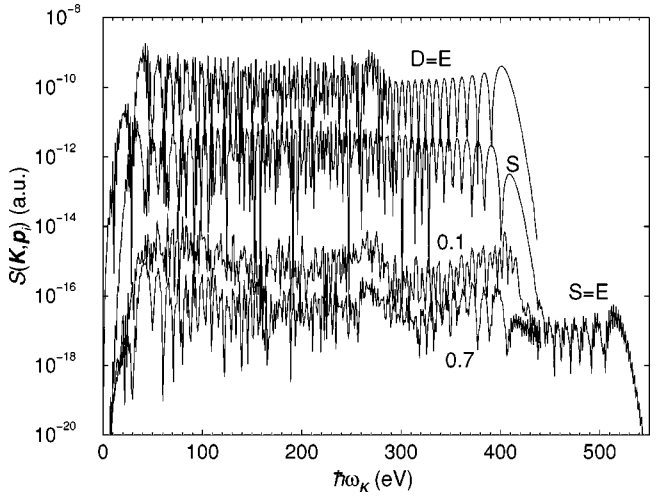

FIG. 5. The differential power spectrum as a function of the emitted x-ray energy for He and a Nd:YAG laser of intensity 1.5×10^{15} W/cm^2 ($U_P=157.3$ eV). The incoming electron energy is three times the laser photon energy. The topmost curve denoted by "$D=E$" refers to the direct LAR process. The curve below it, denoted by "S" represents the data for SLAR only. The lowest curve is also for SLAR and consists of two parts. The left part is composed of two curves denoted by "0.1" and "0.7" (see text for explanation). The second part (for larger x-ray energies) is denoted by "$S=E$" and for this part of the spectrum the direct LAR process disappears so that the SLAR results presented are exact.

It is also interesting that for the value of the incident electron energy chosen above, there is no SLAR spectrum beyond the classical boundaries of the direct LAR process. We postpone the discussion of these results until the next section.

In Fig. 4 we present the results for $E_{\mathbf{p}_i}=72$ eV corresponding to the maximum of the total power presented in Fig. 1 as a function of $E_{\mathbf{p}_i}$ for the laser field intensity 10^{14} W/cm^2. The other parameters are the same as in Fig. 3. Here the results are presented on a logarithmic scale. The results for the direct LAR are shown by a solid line, while the results for SLAR alone are presented by a dotted line with filled diamonds. The SLAR results are now lower by one order of magnitude in the central part of the spectrum, while this difference is larger at the classical boundaries ($28.9\text{ eV}\leqslant\hbar\omega_{\mathbf{K}}\leqslant184$ eV). In order to check whether the short travel times τ are important, we have calculated the differential power spectrum, using Eq. (14) with the lower limit of the integral over τ to be equal to $0.3T$ instead of 0. We found that the SLAR differential power spectrum decreases by four orders of magnitude in comparison with the exact one (with the lower limit $\tau=0$). In this way we artificially excluded the short-travel-time contribution and found that the difference between the probabilities of the direct and the rescattering processes is more than five orders of magnitude. Such a difference one can also expect from the considerations of HATI [22–28].

Finally, in Fig. 5 we present the differential power spectrum as a function of the emitted x-ray energy for He, using a Nd:YAG laser of intensity 1.5×10^{15} W/cm^2, and for the incoming electron energy $E_{\mathbf{p}_i}=3\hbar\omega=3.51$ eV. The highest curve corresponds to the direct LAR process. We denoted it by "$D=E$," where "D" stands for "direct" and "E" stands for "exact," because in the corresponding region of values of $\hbar\omega_{\mathbf{K}}$ the contribution of the SLAR process (the curve denoted by "S" and located below the "$D=E$" curve) is two orders of magnitude smaller and can be neglected. The bottom curves correspond to SLAR only. On the left side we have two curves denoted by "0.1" and "0.7." These curves correspond to the SLAR results obtained by numerical integration over the times $\tau>0.1T$ and $\tau>0.7T$ in Eq. (14), respectively. Comparing these results with the central "S" curve that is 3–5 orders of magnitude higher and includes exact integration ($\tau\geqslant0$), we conclude that the main contribution to this part of the SLAR spectrum comes from the short travel times. The second part of this bottom curve (for larger x-ray energies) is denoted by "$S=E$." In this region the contribution of the direct LAR process to the spectrum is zero, so that only the SLAR part remains and that is why it is denoted as the exact result (it also includes the exact integration). The cutoff position of this part of the spectrum, as well as its characteristic oscillatory structure that is superimposed by the zigzag oscillations, will be explained in the following section.

V. SEMICLASSICAL ANALYSIS

In this section we will explain the numerical results presented in the preceding section using a semiclassical analysis. By semiclassical analysis we mean, in the present context, the analysis of the equations obtained by applying the saddle-point method in order to solve the integrals in the quantum-mechanical expression for the S matrix. The saddle-point equations are obtained by setting the first derivatives equal to zero with respect to the intermediate electron momenta [$\hbar\mathbf{q}$ in Eq. (11)], the initial time t, and the travel time τ, of the expression that appears in the exponential part of the S-matrix element. This method was successfully applied

to HHG and HATI ([19–21] and references therein) where it was used in order to be able to replace a five-dimensional integral by a sum over the relevant saddle points. Due to the tunneling nature of HHG and HATI, in these problems only complex solutions of the saddle-point equations were possible. However, in spite of the fact that the SLAR process also belongs to the class of the three-step processes, in this case there are real solutions. The analysis of real solutions can be considered in classical terms, because in this case a connection with the conservation of classically given energies and the classical equation of motion can be established, as we shall see below.

For the direct LAR process we have only one integral over the time t. The corresponding saddle-point equation is equivalent to the energy-conserving condition at the recombination time t,

$$\frac{1}{2m}[\mathbf{p}_i+e\mathbf{A}(t)]^2=E_B+\hbar\omega_{\mathbf{K}}, \tag{17}$$

i.e., the classical electron kinetic energy in the laser field at time t has to be equal to the energy of the ground state, into which the electron recombines, plus the emitted x-ray energy. We are considering the case $\hbar\omega_{\mathbf{K}}+E_B>0$ for which Eq. (17) has real solutions for t. These solutions depend on the parameter [14] $p_i/(eA_0)=[E_{\mathbf{p}_i}/(2U_P)]^{1/2}$, $A_0=E_0/\omega$. In Fig. 6 these solutions are presented for $0\leqslant t\leqslant 2T$ by stars and denoted by the letter D. One can see that for $p_i>eA_0$, for a fixed value of $(\hbar\omega_{\mathbf{K}}+E_B)/U_P$, there are only two solutions per optical cycle. This means that the main contribution to the integral over time t in the S-matrix element, for a given emitted x-ray energy $\hbar\omega_{\mathbf{K}}$, comes from two different times $t=t_s$, $s=1,2$. These two contributions interfere giving a characteristic oscillatory behavior of the differential power spectrum (see the curve in the middle of Fig. 3 and the upper curve in Fig. 4). Another feature that can be inferred from the D curve in the top panel of Fig. 6 is the classically allowed range of values of $\hbar\omega_{\mathbf{K}}$. There is a maximum that corresponds to Eq. (1) and a minimum that corresponds to the value given by Eq. (1) with a minus sign in front of the square root. The panel in the middle of Fig. 6 corresponds to the boundary case where this minimum energy is $\hbar\omega_{\mathbf{K}}=|E_B|$. For the lower panel in Fig. 6 we have $p_i=0.1eA_0$ and this case corresponds to the ''slow electron'' regime $p_i<eA_0$ [14]. In this case there are two possibilities. For higher values of $\hbar\omega_{\mathbf{K}}$ there are two solutions for t near the maximum at $t=T/2$ and only two electron trajectories [19–21] give the main contribution. However, for the lower values of $\hbar\omega_{\mathbf{K}}$ there are four solutions (two near the maximum at $t=T/2$ as before, and two near the lower maximum at $t=T$). These four solutions are responsible for a complicated interference structure. Using the above analysis it is possible to explain the direct LAR result presented by the upper $D=E$ curve in Fig. 5. For higher values of $\hbar\omega_{\mathbf{K}}$ (276 eV$\leqslant\hbar\omega_{\mathbf{K}}\leqslant$409 eV) there are only two solutions of Eq. (17) for the time t. The interference of the contributions of these two times gives the presented oscillatory spectrum. The lower boundary (276 eV) represents only the boundary for the existence of two real solutions that lead to a simple interference structure in this region. There are four classical solutions for $\hbar\omega_{\mathbf{K}}<276$ eV yielding a more complicated interference pattern as can be seen in Fig. 5.

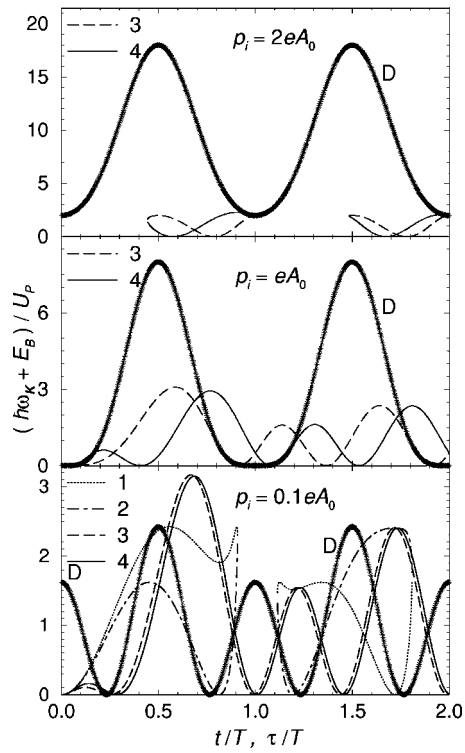

FIG. 6. Real solutions of the semiclassical equations (17)–(22). The sum of the emitted x-ray energy and atomic binding energy divided by the ponderomotive energy $[(\hbar\omega_{\mathbf{K}}+E_B)/U_P]$ is presented as a function of the recombination time t (divided by the laser field period T) for the solution of the Eq. (17) for direct LAR (curves denoted by *''D''*) or as a function of the travel time τ (divided by T) for SLAR (dotted, dotted-dashed, dashed, and solid curves). Top panel corresponds to the case in which the modulus of the incoming electron momentum p_i is equal to $2eA_0$ ($A_0=E_0/\omega$ is the amplitude of the vector potential of the laser field), while the central and the lower panels are for $p_i=eA_0$ and $p_i=0.1eA_0$, respectively. The four solutions for SLAR are marked by numbers (see text for explanation).

Let us now consider the SLAR process. In this case the S-matrix element (11) is presented in the form of a five-dimensional integral. Using the saddle-point method and putting the first derivatives of the exponential term in Eq. (11) with respect to t, τ, and $\hbar\mathbf{q}$, respectively, equal to zero, we obtain

$$\frac{1}{2m}[\mathbf{p}_s+e\mathbf{A}(t)]^2=\frac{1}{2m}[\mathbf{p}_i+e\mathbf{A}(t)]^2, \tag{18}$$

$$\int_t^{t+\tau}dt'[\mathbf{p}_s+e\mathbf{A}(t')]=\mathbf{0}, \tag{19}$$

$$E_B+\hbar\omega_{\mathbf{K}}=\frac{1}{2m}[\mathbf{p}_s+e\mathbf{A}(t+\tau)]^2. \tag{20}$$

Equation (18) represents the energy conservation at time t for the laser-assisted scattering of the electron having initial mo-

mentum $\mathbf{p}_i$. The condition for the electron to return to the ion after the travel time τ is given by Eq. (19). For real solutions this condition can be obtained by solving the classical equation of motion for the electron in the laser field: $m\ddot{\mathbf{r}}=-e\mathbf{E}_L(t)$. Equation (19) also defines the stationary momentum $\hbar\mathbf{q}=\mathbf{p}_s$. Finally, Eq. (20) expresses the energy conservation at the recombination time $t+\tau$. This system of equations for the saddle points $(\mathbf{p}_s,t_s,\tau_s)$ is very similar to that presented in [19–21] for HHG and HATI. The difference is that for $\hbar\omega_{\mathbf{K}}\geqslant|E_B|$ our system has real solutions that simplify the analysis.

In order to find the real solutions of the system (18)–(20) we will first simplify it taking into account that in our case the incident electron momentum $\mathbf{p}_i$ is antiparallel to our linearly polarized laser field. Then, after the substitution of $\mathbf{p}_s$ from Eq. (19) into Eqs. (18) and (20), we obtain a system of two equations for t and τ. Introducing the variable $\sigma=\omega\tau/2$ and the notation $s(\sigma)=\sin\sigma$, $c(\sigma)=\cos\sigma-s/\sigma$, $x=\cos(\omega t+\sigma)$, $y=\sin(\omega t+\sigma)$, $p=p_i/(eA_0)$, this system reduces to

$$cx+sy=\pm(x\cos\sigma+sy-p), \tag{21}$$

$$(\hbar\omega_{\mathbf{K}}+E_B)/U_P=2(cx-sy)^2. \tag{22}$$

Equation (21) corresponds to the energy-conserving condition (18), where the square root on both sides of this equation was taken, while Eq. (22) stems from Eq. (20). Using Eq. (21) we can express the variables x and y in terms of the variable $\sigma=\omega\tau/2$. Introducing these solutions for x and y into Eq. (22) we obtain an equation that expresses the emitted x-ray energy as a function of the travel time τ. These solutions are presented in Fig. 6 by the dotted, dotted-dash, dashed, and solid lines, and will be analyzed below. Under certain restrictions on the parameter $p=p_i/(eA_0)$, the system (21)–(22) has two real solutions for the "+" sign in Eq. (21) and two real solutions for the "−" sign. For the "+" sign in Eq. (21) we find $x=p\sigma/s$, so that $y=\pm\sqrt{1-(p\sigma/s)^2}$ and we have two real solutions for $(\hbar\omega_{\mathbf{K}}+E_B)/U_P$ as a function of τ as long as $p<1$. The condition $p<1$ is equivalent to $E_{\mathbf{p}_i}<2U_P$ so that these two real solutions, which we shall denote by 1 and 2, only exist for low incoming electron energies. For the "−" sign in Eq. (21) we have another pair of solutions that we denote by 3 and 4. We shall again express the variables x and y through σ and insert them into Eq. (22). The resulting quadratic equation in terms of the variable x has the real solutions

$$x=[p(c+\cos\sigma)\pm 2s\sqrt{b-p^2}]/b,$$

$$b(\sigma)=(c+\cos\sigma)^2+4s^2, \tag{23}$$

if $b\geqslant p^2$. We therefore have again obtained a restriction on the values of the parameter p under which real solutions exist. The maximum value of p for which the condition $p^2=E_{\mathbf{p}_i}/(2U_P)\leqslant b$ is satisfied can be determined from the condition $\partial b/\partial\sigma=0$. We find the following nonlinear equation for σ:

$$\left(\frac{1}{\sigma}-\cot\sigma\right)\left(\frac{1}{2\sigma}-\cot\sigma\right)=1.$$

By introducing the solution σ_0 of this equation back into the initial inequality $p^2\leqslant b(\sigma_0)$, we obtain the condition $E_{\mathbf{p}_i}\leqslant 10.007U_P$. Therefore, the maximum of the classically allowed value of the incident electron kinetic energy is $E_{\mathbf{p}_i}=10.007U_P$, which is the same result as the known cutoff law for HATI: $E_{\mathbf{p}_i}=10.007U_P$ (see [22–28], and also [41]). This classical cutoff law for HATI was obtained by assuming that the atomic binding energy is equal to zero so that real solutions were possible. In our case, this upper limit on the allowed incoming electron energy can be understood in the following way. If the incident electron energy is too large, then, after the rescattering, the laser field will not be able to push the electron back to the nucleus and the electron will move away and hence the recombination process will not be possible. We conclude that, irrespective of the electron incident energy and of the instant of time of recollision, for $E_{\mathbf{p}_i}>10.007U_P$ the SLAR process is classically forbidden. Of course, quantum mechanically the SLAR process is possible also for $E_{\mathbf{p}_i}>10.007U_P$, as it can be seen from the results presented in Figs. 3 and 4. This can be explained by the existence of complex solutions of the semiclassical equations (18)–(20).

With these results, let us now analyze the numerical results presented in Fig. 6. For values of $E_{\mathbf{p}_i}$ lower than $10.007U_P$, the real solutions of the system (21)–(22) exist, as can be seen in the top panel ($p_i=2eA_0$, i.e., $E_{\mathbf{p}_i}=8U_P$) of Fig. 6 where the solutions 3 and 4 start to appear. The corresponding x-ray energies are much lower than those of the direct LAR x rays (the curve marked with D). For the panel in the middle ($p_i=eA_0$, i.e., $E_{\mathbf{p}_i}=2U_P$) the solutions 3 and 4 are well developed and the corresponding x-ray energies are of the order of $3U_P$, but they are still lower than those of the direct LAR process. Finally, in the bottom panel, which corresponds to $p_i=0.1eA_0$, i.e., to $E_{\mathbf{p}_i}=0.02U_P$, we see that the highest x-ray energy is that of the solutions 3 and 4 and it approaches $3.17U_P+|E_B|$, the cutoff of HHG. These results refer to the numerical data denoted by $S=E$ in Fig. 5. The curves that correspond to the solutions 3 and 4 as functions of τ are close to each other so that the superposition of their oscillations produces the characteristic shape of this $S=E$ part in Fig. 5. The solutions 1 and 2 also exist in this case and they are presented by dotted and dotted-dash lines in the bottom panel of Fig. 6. There are two broad maxima, the higher of which is of the same height as the maximum of the D curve for the direct LAR process. For values of τ near T there is a band in which the solutions 1 and 2 are absent.

The system (18)–(20) has also complex solutions. According to our knowledge about HHG and HATI we expect that the contribution of these solutions with large imaginary parts is small. For example, for HHG by an elliptically polarized laser field [19,21,42] or HHG in a relativistically strong field (such that the $\mathbf{v}\times\mathbf{B}$ drift is large [43]), the imaginary parts of these solutions become large, so that HHG is

highly suppressed. However, the SLAR process is different in the sense that one has available initially the incoming electron energy. In this case, for short travel times τ, the system (18)–(20) can have complex solutions that give an important contribution. For example, for the results presented in Fig. 3, the SLAR process is classically forbidden since the parameter $p_i/(eA_0)=3.089>\sqrt{5}$, where the factor $\sqrt{5}\approx 2.237$ originates in the cutoff law at $10.007U_P$. Nevertheless, the corresponding power spectrum (the bottom curve) is only slightly lower than the one of the direct LAR process (the middle curve), so that their interference is clearly visible in the total power spectrum (the top curve). These results can be explained by the existence of the complex solutions of the saddle-point equations for short travel times. The electrons that are scattered in the backward direction will start to move in the direction of the polarization vector of the laser field. It is possible that after a very short travel time the electrons are still in the vicinity of the nucleus so that they can recombine with a high probability. There is an indication that this mechanism is responsible for the large SLAR results. Namely, the SLAR curve has its maxima at the same positions where the direct LAR curve has its minima, as seen in Fig. 3. It may well be that for the direct LAR and for the SLAR process the electron follows the laser field oscillations in opposite directions. Another example of the importance of the complex solutions are the results presented in Fig. 4. For the parameters of this figure, the real solutions of Eqs. (18)–(22) exist because $p_i=1.853eA_0$. However, the cutoff for these solutions, which are analogous to the solutions 3 and 4 presented in the top panel of Fig. 6, yields $0<\hbar\omega_{\mathbf{K}}\leqslant|E_B|+2.45U_P=39.3$ eV. Therefore, in this case, similarly to Fig. 3, the contribution of the nonclassical complex solutions is dominant.

Finally, it is interesting that the $S=E$ part of the spectrum in Fig. 5 can be explained by the real solutions of the semiclassical equations (18)–(20). Referring to the bottom panel of Fig. 6, we see that in this spectral region only the solutions 3 and 4 exist (dashed and solid lines). They lead to the cutoff for the SLAR process at $\hbar\omega_{\mathbf{K}}=|E_B|+3.17U_P=523$ eV. Solutions 3 and 4 are close to each other and, for a fixed value of the emitted x-ray photon energy, there are four solutions for $0\leqslant\tau\leqslant T$ that interfere, resulting in a characteristic oscillatory structure that is superimposed by the zigzag oscillations.

VI. CONCLUSIONS

The study of the laser-assisted electron-ion recombination that includes the scattering of the electron at the ion prior to its recombination is important due to the two following main reasons. (i) As we have mentioned in the introduction, the laser-assisted electron-ion recombination could be another potential source for generating coherent soft x rays and thus further information about this process will be useful in achieving this goal. In the present work, we have shown that the recombination process is more important for lower incident electron energies and that, for a given high-intensity laser field, the total power of the emitted x rays as a function of the incident electron energy has its maximum if the incident electron energy is equal to a few times the ponderomotive energy. (ii) In our opinion, however, the more important reason for our investigation is the existing complementarity between our process and the well-known HHG and HATI. In fact, all of them can be explained by using the three-step model. This implies the use of a similar theoretical formalism that is based on the *S*-matrix theory and on the semiclassical saddle-point solutions. Equivalently, it can also be formulated by using the Feynman path integrals [20]. An important difference is, however, that HHG and HATI are genuinely tunneling phenomena, whereas our SLAR process has in its initial state a free electron with a positive energy. Therefore, we have only complex solutions of the saddle-point equations for HHG and HATI, while for SLAR also real solutions are possible. Using these real solutions, we were able to derive two cutoff laws for SLAR. One concerns the maximum incident electron energy for which the SLAR process is ''classically'' still possible. It is the same $10.007U_P$ cutoff law as that for the maximum outgoing electron energy in HATI [22–28,41]. The second cutoff law determines the maximum energy of the emitted soft x rays in SLAR, and it is the same $|E_B|+3.17U_P$ cutoff law as for HHG [9]. However, the SLAR saddle-point equations have also complex solutions. Their contribution becomes important for short electron travel times. Therefore, the $10.007U_P$ cutoff law is only classically valid but it is not a real limitation on the values of the incident electron energy, as is confirmed by our numerical calculations. Concerning the cutoff law for the high-energy photons, our results show that it is given by the formula $\hbar\omega_{\mathbf{K},\max}=|E_B|+\max\{3.17U_P, E_{\mathbf{p}_i}+2U_P+2\sqrt{2E_{\mathbf{p}_i}U_P}\}$. The second term in this curly brackets is identical to what is found for the direct LAR cutoff law, as shown in by Eq. (1). For SLAR it corresponds to the complex solutions mentioned before. It is important that the probabilities of SLAR that belong to these solutions and for short travel times are much higher than expected. Namely, the ratio of the rates of the direct and the rescattering process (for HATI, for example) is usually about 10^6–10^7. We can infer, however, from Figs. 3–5 that in our problem this ratio is only 10–100 or even less. As we have mentioned in Sec. V, one possible explanation for this result is that the backscattered electron recombines with a high probability immediately after the scattering event has taken place and when it is still in the vicinity of the nucleus. One can speculate whether in the case where the direct recombination process is not allowed (due to selection rules, for example) or is highly suppressed, SLAR presents a new channel for the energy transfer of the incoming electrons to the high-energy photons. The short-travel-time transfer mechanism is not characteristic of SLAR only. There is an indication (D. B. Milošević, unpublished) that for the short travel times additional complex solutions (in comparison to those presented in Refs. [19,21]) of the saddle-point equations for HHG exist, the contribution of which to the low-energy part of the spectrum may be important. We expect a similar behavior in the case of HATI. For HHG it may be connected to the so-called nontunneling harmonics [44].

ACKNOWLEDGMENTS

The authors wish to thank Dr. W. Becker for useful comments. This work was supported by a Special Research Project for 2000–2001 of the Office for Scientific-Technical Collaboration of the Austrian Academic Exchange Services. D.B.M. also gratefully acknowledges support by the VolkswagenStiftung.

[1] M. H. Mittleman, *Introduction to the Theory of Laser-Atom Interactions*, 2nd ed. (Plenum, New York, 1993).

[2] L. F. DiMauro and P. Agostini, Adv. At., Mol., Opt. Phys. **35**, 79 (1995).

[3] M. Protopapas, C. H. Keitel, and P. L. Knight, Rep. Prog. Phys. **60**, 389 (1997).

[4] C. J. Joachain, M. Dörr, and N. Kylstra, Adv. At., Mol., Opt. Phys. **42**, 225 (2000).

[5] M. Drescher, M. Hentschel, R. Kienberger, G. Tempea, Ch. Spielmann, G. A. Reider, P. B. Corkum, and F. Krausz, Science **291**, 1923 (2001).

[6] P. M. Paul, E. S. Toma, P. Breger, G. Mullot, F. Augé, Ph. Balcou, H. G. Muller, and P. Agostini, Science **292**, 1689 (2001).

[7] See references in D. B. Milošević and W. Sandner, Opt. Lett. **25**, 1532 (2000), on the importance of the generation of coherent radiation near 13 nm for extreme-ultraviolet lithography that is a leading candidate as a technology for fabricating 0.1-μm generation of integrated circuit.

[8] See D. B. Milošević and A. F. Starace, Phys. Rev. Lett. **81**, 5097 (1998); Laser Phys. **10**, 278 (2000), and references therein, for the possibilities of generating coherent x-ray photons with energies in the ''water window'' [between the *K*-shell absorption edges of carbon (284 eV, 4.37 nm) and oxygen (532 eV, 2.33 nm)] and possible applications.

[9] P. Salières, A. L'Huillier, Ph. Antoine, and M. Lewenstein, Adv. At., Mol., Opt. Phys. **41**, 83 (1999).

[10] T. Brabec and F. Krausz, Rev. Mod. Phys. **72**, 545 (2000).

[11] F. Ehlotzky, A. Jaroń, and J. Z. Kamiński, Phys. Rep. **297**, 63 (1998).

[12] D. B. Milošević and F. Ehlotzky, Phys. Rev. A **58**, 2319 (1998); D. B. Milošević and A. F. Starace, J. Phys. B **32**, 1831 (1999); Phys. Rev. A **60**, 3943 (1999).

[13] A. Jaroń, J. Z. Kamiński, and F. Ehlotzky, Phys. Rev. A **61**, 023404 (2000); **63**, 055401 (2001); Laser Phys. **11**, 174 (2001); J. Phys. B **34**, 1221 (2001).

[14] M. Yu. Kuchiev and V. N. Ostrovsky, Phys. Rev. A **61**, 033414 (2000); J. Phys. B **34**, 405 (2001) (see Appendix B about LAR in the context of HHG).

[15] Y. Hahn, Rep. Prog. Phys. **60**, 691 (1997).

[16] For an extended list of references see [13–15]. We add here a theoretical paper on resonant recombination: L. Rosenberg, Phys. Rev. A **51**, 3676 (1995); papers on recombination in a pulsed electric field: T. J. Bensky, M. B. Campbell, and R. R. Jones, Phys. Rev. Lett. **81**, 3112 (1998); C. Wesdorp, F. Robicheaux, and L. D. Noordam, *ibid.* **84**, 3799 (2000); Phys. Rev. A **64**, 033414 (2001); and a paper on polarization recombination: L. Bureyeva and V. Lisitsa, J. Phys. B **31**, 1477 (1998). More recently, the influence of crossed electric and magnetic fields on dielectronic recombination has been measured: S. Böhm, S. Schippers, W. Shi, A. Müller, N. Djurić, G. H. Dunn, W. Zong, B. Jelenković, H. Danared, N. Eklöw, P. Glans, and R. Schuch, Phys. Rev. A **64**, 032707 (2001).

[17] Stimulated emission of high harmonics was analyzed in the context of amplification of high-order harmonics in: E. A. Nersesov, S. V. Popruzhenko, D. F. Zaretsky, W. Becker, and P. Agostini, Phys. Rev. A **64**, 023419 (2001).

[18] K. C. Kulander, K. J. Schafer, and J. L. Krause, in *Super-Intense Laser-Atom Physics*, Vol. 316 of *NATO Advanced Study Institute, Series B: Physics*, edited by B. Piraux, A. L'Huillier, and K. Rzążewski (Plenum, New York, 1993); P. B. Corkum, Phys. Rev. Lett. **71**, 1994 (1993); see also: M. Yu. Kuchiev, Pis'ma Zh. Éksp. Teor. Fiz. **45**, 319 (1987) [JETP Lett. **45**, 404 (1987)].

[19] R. Kopold, D. B. Milošević, and W. Becker, Phys. Rev. Lett. **84**, 3831 (2000).

[20] P. Salières, B. Carré, L. Le Déroff, F. Grasbon, G. G. Paulus, H. Walther, R. Kopold, W. Becker, D. B. Milošević, A. Sanpera, and M. Lewenstein, Science **292**, 902 (2001).

[21] R. Kopold, W. Becker, and D. B. Milošević, J. Mod. Opt. (to be published).

[22] K. J. Schafer, B. Yang, L. F. DiMauro, and K. C. Kulander, Phys. Rev. Lett. **70**, 1599 (1993); B. Yang, K. J. Schafer, B. Walker, K. C. Kulander, P. Agostini, and L. F. DiMauro, *ibid.* **71**, 3770 (1993).

[23] G. G. Paulus, W. Nicklich, H. Xu, P. Lambropoulos, and H. Walther, Phys. Rev. Lett. **72**, 2851 (1994); G. G. Paulus, W. Nicklich, and H. Walther, Europhys. Lett. **27**, 267 (1994); G. G. Paulus, W. Nicklich, F. Zacher, P. Lambropoulos, and H. Walther, J. Phys. B **29**, L249 (1996).

[24] B. Walker, B. Sheehy, K. C. Kulander, and L. F. DiMauro, Phys. Rev. Lett. **77**, 5031 (1996).

[25] M. Lewenstein, K. C. Kulander, K. J. Schafer, and P. H. Bucksbaum, Phys. Rev. A **51**, 1495 (1995).

[26] W. Becker, A. Lohr, and M. Kleber, J. Phys. B **27**, L325 (1994); **28**, 1931 (1995); A. Lohr, M. Kleber, R. Kopold, and W. Becker, Phys. Rev. A **55**, R4003 (1997); G. G. Paulus, F. Zacher, H. Walther, A. Lohr, W. Becker, and M. Kleber, Phys. Rev. Lett. **80**, 484 (1998).

[27] D. B. Milošević and F. Ehlotzky, Phys. Rev. A **57**, 5002 (1998).

[28] D. B. Milošević and F. Ehlotzky, Phys. Rev. A **58**, 3124 (1998); J. Phys. B **31**, 4149 (1998); **32**, 1585 (1999).

[29] C. J. Joachain, *Quantum Collision Theory* (North-Holland, Amsterdam, 1975).

[30] In the HATI process there are no x-ray photons in the initial state and it also includes the tunneling process so that the semiclassical analysis includes complex quantities [19,20].

[31] D. B. Milošević, in *Super-Intense Laser-Atom Physics*, edited by B. Piraux and K. Rzążewski (Kluwer, Netherlands, 2001), p. 229.

[32] W. Becker, A. Lohr, M. Kleber, and M. Lewenstein, Phys. Rev. A **56**, 645 (1997).
[33] L. V. Keldysh, Zh. Éksp. Teor. Fiz. **47**, 1945 (1964) [Sov. Phys. JETP **20**, 1307 (1965)]; F. H. M. Faisal, J. Phys. B **6**, L89 (1973); H. R. Reiss, Phys. Rev. A **22**, 1786 (1980).
[34] H. R. Reiss, Phys. Rev. A **42**, 1476 (1990); Prog. Quantum Electron. **16**, 1 (1992).
[35] M. Lewenstein, Ph. Balcou, M. Yu. Ivanov, A. L'Huillier, and P. B. Corkum, Phys. Rev. A **49**, 2117 (1994).
[36] D. B. Milošević and B. Piraux, Phys. Rev. A **54**, 1522 (1996).
[37] A. A. Radzig and B. M. Smirnov, *Reference Data on Atoms, Molecules and Ions* (Springer, Berlin, 1985).
[38] B. Hüpper, J. Main, and G. Wunner, Phys. Rev. Lett. **74**, 2650 (1995); Phys. Rev. A **53**, 744 (1996).
[39] D. B. Milošević and F. Ehlotzky, Laser Phys. **9**, 149 (1999).
[40] G. F. Drukarev, *The Theory of Electron-Atom Collisions* (Academic, London, 1965).
[41] G. G. Paulus, W. Becker, and H. Walther, Phys. Rev. A **52**, 4043 (1995).
[42] D. B. Milošević, J. Phys. B **33**, 2479 (2000).
[43] D. B. Milošević, S. Hu, and W. Becker, Phys. Rev. A **63**, 011403(R) (2001); Laser Phys. **12**, 389 (2002).
[44] S. X. Hu, D. B. Milošević, W. Becker, and W. Sandner, Phys. Rev. A **64**, 013410 (2001); S. X. Hu, A. F. Starace, W. Becker, W. Sandner, and D. B. Milošević, J. Phys. B **35**, 627 (2002).